

The Fisher Paradox: Dissipation Interference in Information-Regularized Gradient Flows

Michael Farmer,¹ Abhinav Kochar,¹ and Yugyung Lee¹

¹University of Missouri–Kansas City

(Dated: March 16, 2026)

We show that Fisher-regularized Wasserstein gradient flows exhibit a previously unrecognized interference mechanism in their dissipation identity: a cross-dissipation term whose sign becomes positive when the state width falls below a critical scale. In this regime the geometric Fisher channel transiently opposes descent of the baseline free-energy functional, producing what we term the *Fisher Paradox*. Restricting the flow to the Gaussian manifold yields an exact Riccati-type variance equation with a closed-form trajectory, exposing three dynamical regimes separated by two critical scales: $\sigma = 1$ (cross-dissipation sign flip) and $\sigma = \sqrt{\varepsilon}$ (Fisher takeover). The variance potential $V(u) = u^2 - 2u - \varepsilon \ln u$ contains a logarithmic centrifugal barrier that shifts the equilibrium attractor by $\Delta\sigma \approx \varepsilon/4$. The interference persists for a duration $t_{\text{cross}} \sim D_{\text{KL}}$, linking the dissipation delay directly to initial information distance. Finite-difference simulations on a 512-point grid confirm all analytical predictions to within 5.21×10^{-4} mean relative error. Numerical experiments with bimodal and Laplace initial conditions confirm the effect persists beyond Gaussian closure, with direct implications for information-geometric dissipative dynamics.

INTRODUCTION

Wasserstein gradient flows provide the geometric foundation for a large class of dissipative systems [1–3]:

$$\partial_t \rho = \nabla \cdot (\rho \nabla \mu), \quad \mu = \frac{\delta \mathcal{F}}{\delta \rho}. \quad (1)$$

A common modification introduces Fisher information regularization. We use the convention $\Phi_F(\rho) = \int |\nabla \sqrt{\rho}|^2 dx = \frac{1}{4} I(\rho)$, where $I(\rho) = \int \rho |\nabla \log \rho|^2 dx$ is the standard Fisher information [4, 5]. The regularized functional is

$$\mathcal{F}_\varepsilon(\rho) = \mathcal{F}_0(\rho) + \varepsilon \Phi_F(\rho). \quad (2)$$

Although \mathcal{F}_ε decreases monotonically, we show that its dissipation identity contains a cross-term whose sign depends on the state width σ : when $\sigma < 1$ the geometric Fisher channel transiently opposes free-energy descent of the *baseline* functional \mathcal{F}_0 . We call this the **Fisher Paradox**: additive geometric regularization retards free-energy descent during a well-defined transient window. The effect is not simply a consequence of changing the objective: it appears explicitly in the dissipation identity for \mathcal{F}_0 , the regularized system settles to a *permanently* shifted attractor $\sigma_\infty = 1 + \varepsilon/4 \neq \sigma_\infty^{(0)} = 1$, and the retardation duration is set by the initial information distance—all absent from unregularized flow.

We work with the canonical Ornstein–Uhlenbeck (OU) free energy $\mathcal{F}_0(\rho) = \int \rho \ln \rho dx + \frac{1}{2} \int x^2 \rho dx$, whose Wasserstein flow preserves Gaussian structure, enabling an exact analytical reduction to a single variance ODE. The three-regime structure and KL scaling law are derived exactly within the Gaussian manifold; the sign competition in Eq. (8) does not depend on Gaussian closure, as confirmed numerically for bimodal and Laplace initial conditions.

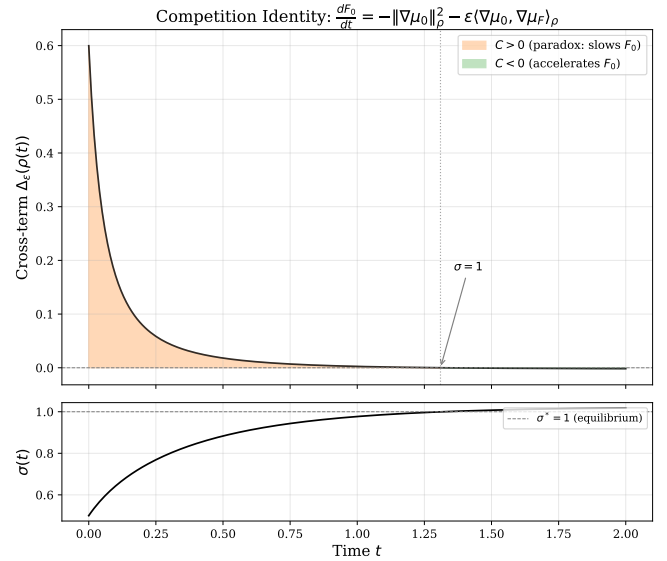


FIG. 1. Cross-term $\Delta_\varepsilon(\rho(t))$ (top) and variance $\sigma(t)$ (bottom) for $\varepsilon = 0.1$, $\sigma_0 = 0.5$. The cross-term is positive (orange) while $\sigma < 1$, slowing \mathcal{F}_0 decay; the sign changes at $\sigma = 1$ (dotted). $\sigma(t)$ relaxes toward $\sigma^* \approx 1 + \varepsilon/4$.

RICCATI REDUCTION AND EXACT TRAJECTORY

Adding Fisher regularization modifies the chemical potential to $\mu_\varepsilon = \mu_0 + \varepsilon \mu_F$ with $\mu_0 = \ln \rho + x^2/2$ and

$$\mu_F = \frac{\delta \Phi_F}{\delta \rho} = -\frac{\Delta \sqrt{\rho}}{\sqrt{\rho}}. \quad (3)$$

The complete derivation is given in Supplemental Sec. A; the two factors of 2 cancel, yielding no prefactor. For Gaussian states $\rho_\sigma(x) = (2\pi\sigma^2)^{-1/2} \exp(-x^2/2\sigma^2)$, one

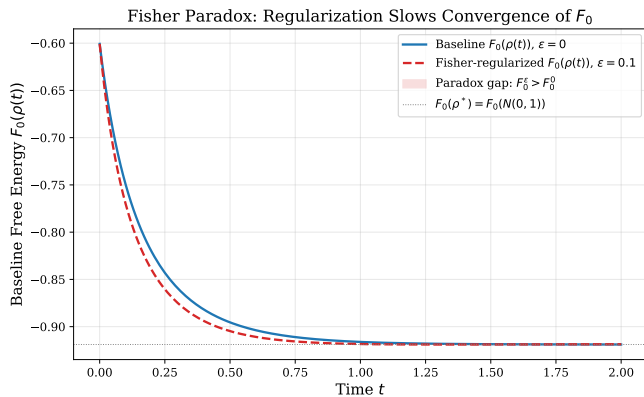


FIG. 2. Baseline free energy $\mathcal{F}_0(\rho(t))$ with ($\varepsilon = 0.1$, dashed red) and without ($\varepsilon = 0$, solid blue) regularization. The paradox gap (pink shading) confirms transient retardation; both curves converge to $\mathcal{F}_0(\mathcal{N}(0, 1))$ (dotted).

computes $\mu_F = (2\sigma^2 - x^2)/(4\sigma^4)$, and the variance moment equation yields the σ -ODE

$$\dot{\sigma} = \frac{1 - \sigma^2}{\sigma} + \frac{\varepsilon}{2\sigma^3}. \quad (4)$$

Setting $u = \sigma^2$ removes the singularity:

$$\dot{u} = 2(1 - u) + \frac{\varepsilon}{u}. \quad (5)$$

Equation (5) is separable with roots $u_{\pm} = (1 \pm \sqrt{1 + 2\varepsilon})/2$, giving the implicit closed-form trajectory

$$t = \frac{u_- \ln|u - u_-| - u_+ \ln|u - u_+|}{2(u_+ - u_-)} + C. \quad (6)$$

For $\varepsilon \rightarrow 0$, Eq. (6) reduces to $t \approx -\frac{1}{2} \ln(1 - u) + \frac{1}{2} u$, recovering standard OU relaxation. For $u_0 \ll 1$, the Fisher-dominant limit gives $t \approx (u^{-1} - u_0^{-1})/(2\varepsilon)$, confirming stiff dynamics near the origin.

THREE-SCALE PHASE STRUCTURE

The reduced system is a gradient flow in the variance potential

$$V(u) = u^2 - 2u - \varepsilon \ln u, \quad (7)$$

encoding OU confinement, entropy, and Fisher curvature respectively. The $-\varepsilon \ln u$ term acts as a *logarithmic centrifugal barrier*, analogous to the centrifugal term in polar-coordinate quantum mechanics and to the Coulomb-gas entropy repulsion in random matrix theory [6]: it prevents variance collapse but forces a mandatory macroscopic overshoot. Two critical scales separate three regimes.

Regime I—Fisher dominance ($\sigma < \sqrt{\varepsilon}$). The Fisher drift $\varepsilon/(2\sigma^3)$ overwhelms the OU drift $1/\sigma$, giving

$\dot{\sigma} \approx \varepsilon/(2\sigma^3)$. This is the *second critical threshold*: below $\sigma \sim \sqrt{\varepsilon}$ the system is numerically stiff, with drift and sensitivity scaling as σ^{-3} and σ^{-4} . Discretized implementations therefore encounter a practical *uncertainty floor* at $\sigma \sim \sqrt{\varepsilon}$, below which curvature regularization governs the effective step size.

Regime II—Competition ($\sqrt{\varepsilon} < \sigma < 1$). The \mathcal{F}_0 dissipation rate splits into

$$\frac{d\mathcal{F}_0}{dt} = - \int \rho \|\nabla \mu_0\|^2 - \varepsilon \int \rho \nabla \mu_0 \cdot \nabla \mu_F. \quad (8)$$

The second term is positive here, producing the Fisher Paradox.

Regime III—Shifted equilibrium ($\sigma > 1$). The fixed point $2u^2 - 2u - \varepsilon = 0$ gives

$$\sigma_{\infty} = \sqrt{u^*} \approx 1 + \frac{\varepsilon}{4}, \quad \Delta\sigma \approx \frac{\varepsilon}{4}. \quad (9)$$

The full energy decomposition ($\mathcal{F}_{\varepsilon}$, \mathcal{F}_0 , and $\varepsilon\Phi_F$ separately) is shown in Supplemental Fig. S2, where $\mathcal{F}_{\varepsilon}$ decreases monotonically while \mathcal{F}_0 experiences transient retardation at $-2.06\times$ the unregularized baseline rate during the competition window.

KL RELAXATION LAW

The paradox persists until $\sigma = 1$; the crossing time is

$$t_{\text{cross}} = \int_{u_0}^1 \frac{u du}{2(u - u^2) + \varepsilon}. \quad (10)$$

For small ε and σ_0 sufficiently below 1, $t_{\text{cross}} \approx \frac{1}{2} \ln(1/\sigma_0^2)$. Since $D_{\text{KL}}(\rho_0 \|\rho^*) \approx -\frac{1}{2} \ln \sigma_0^2$ for $\sigma_0 \ll 1$,

$$\boxed{t_{\text{cross}} \sim D_{\text{KL}}}. \quad (11)$$

The paradox duration equals precisely the initial information distance from equilibrium.

NUMERICAL VALIDATION

We simulated the regularized Fokker-Planck equation on a 512-point grid with semi-implicit operator splitting (Supplemental Sec. S1). The analytical cross-term $C(\sigma) = (1 - \sigma^2)/(2\sigma^4)$ is confirmed to within 5.21×10^{-4} mean relative error (Fig. 3), and full PDE trajectories match the σ -ODE (4) to within 0.2% (Supplemental Sec. S1). Figure 5 shows the paradox gap and cross-term across seven initial conditions $\sigma_0 \in [0.3, 2.0]$, confirming the sign change at $\sigma = 1$ and a monotone increase in paradox amplitude as $\sigma_0 \rightarrow 0$, consistent with the σ^{-4} sensitivity scaling of Regime I.

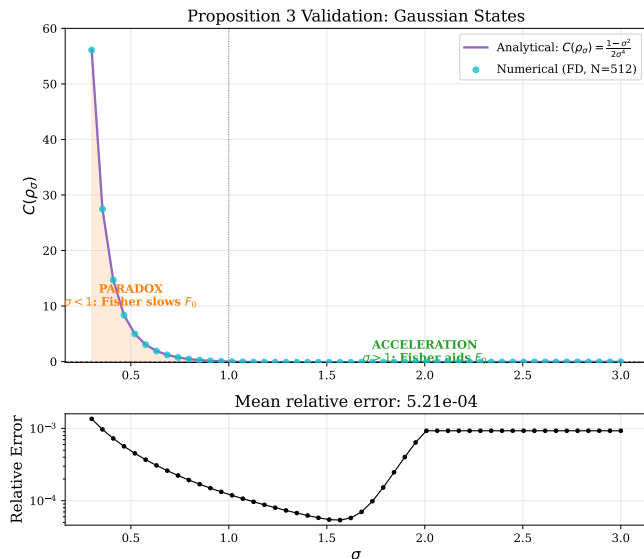


FIG. 3. Validation of $C(\rho_\sigma) = (1 - \sigma^2)/(2\sigma^4)$. *Top*: Analytical (purple) vs. finite-difference (cyan, $N = 512$). Paradox ($\sigma < 1$, orange) and acceleration ($\sigma > 1$, green) regions shown. *Bottom*: Relative error; mean 5.21×10^{-4} .

DISCUSSION

The Fisher Paradox emerges from competition between the $-\varepsilon \ln u$ centrifugal barrier and OU transport, producing stiff anti-collapse below $\sigma \sim \sqrt{\varepsilon}$, the paradox window $(\sqrt{\varepsilon}, 1)$, and the permanently shifted attractor $\sigma_\infty = 1 + \varepsilon/4$. The equilibrium shift is a permanent consequence of the regularization, not merely a transient one: the regularized system settles to a state with strictly higher \mathcal{F}_0 than the unregularized fixed point, a distinction measurable independently of the paradox window. These results are exact on the Gaussian manifold.

Generality of the critical scale. The threshold $\sigma_c = 1$ is specific to $V(x) = x^2/2$. For a general confining potential $V(x)$, the cross-term changes sign where $\mathbb{E}_{\rho_\sigma}[xV'(x)] = 1$, giving $\sigma_c^2 = 1/\mathbb{E}_{\rho_{\sigma_c}}[V''(X)]$ —the reciprocal of the average curvature of V under the state. For $V = x^2/(2L^2)$, $\sigma_c = L$: the paradox window is set by the ratio of state width to the natural equilibrium scale, not by any absolute threshold.

Non-Gaussian universality of t_{cross} . To verify that the mechanism is not restricted to Gaussian closure, we repeated the numerical experiment with non-Gaussian initial conditions matched to the same effective width $\sigma_{\text{eff}} = 0.5$: a symmetric bimodal mixture $\rho_0 = \frac{1}{2}\mathcal{N}(-0.4, 0.09) + \frac{1}{2}\mathcal{N}(0.4, 0.09)$ and a Laplace distribution $\rho_0 \propto e^{-|x|/b}$ with $b = \sigma_{\text{eff}}/\sqrt{2}$. In both cases the cross-dissipation term $C(\rho(t)) = \int \rho \nabla \mu_0 \nabla \mu_F dx$ remains positive throughout $\sigma_{\text{eff}} < 1$ (Fig. 4), producing the same paradox duration $t_{\text{cross}} \approx 1.32$. While non-Gaussian structure modifies the initial magnitude of the cross-term

($\approx 0.56\times$ for the bimodal mixture, $\approx 4\times$ for the Laplace cusp relative to the Gaussian value $C(0) = 6.0$; see Supplemental Table S3), all trajectories converge to the same shifted equilibrium, consistent with a common attractor structure. The preserved t_{cross} is not a coincidence; it follows from a perturbative bound. The variance ODE is $\dot{u} = 2(1 - u) + \varepsilon K(\rho)$, where $K(\rho) = -2 \int x \rho \partial_x \mu_F dx$ is the Fisher variance moment (distinct from the free-energy cross-term C ; for Gaussians $K_G = 1/u$). Writing $K = K_G + \delta K$, integrating against the shape-relaxation decay $|\delta K(\rho(t))| \lesssim |\delta K_0| e^{-2t}$ (OU second eigenvalue), and evaluating at the initial rate $\dot{u}_0 = 2(1 - u_0) + \varepsilon/u_0$ gives

$$|\Delta t_{\text{cross}}| \leq \frac{\varepsilon |\delta K_0|}{2 \dot{u}_0}. \quad (12)$$

For the Laplace IC, $|\delta K_0/K_G| \sim \kappa_4/\sigma^4 \approx 1.5$ ($\kappa_4 = 6b^4$, $b = 0.354$), giving

$$|\Delta t_{\text{cross}}| \leq \frac{0.1 \times (1.5/0.25)}{2 \times 1.90} = 0.079 \approx 6\% \text{ of } t_{\text{cross}}.$$

The bound is conservative: near $u \rightarrow 1$ where the integral weight concentrates, $\dot{u} \rightarrow 0^+$ but the OU shape-relaxation rate ($\lambda_2 = 2$) already dominates, so ρ is near-Gaussian by the time it matters. Full derivation in Supplemental Sec. S6. This strongly indicates that the paradox arises from the sign structure of the dissipation identity, not from Gaussian closure (see Supplemental Secs. S1–S6).

The KL scaling law (11) gives a thermodynamic interpretation independent of system parameters: paradox duration equals the information the system must dissipate before diffusive relaxation dominates.

Connections to existing literature. The functional derivative $\mu_F = -\Delta\sqrt{\rho}/\sqrt{\rho}$ is precisely the quantum pressure (Bohm potential) of Madelung’s hydrodynamic formulation of quantum mechanics [7, 8]; retardation effects of the quantum pressure on classical probability flows have been noted in that context. The present analysis provides a clean dissipation-identity mechanism for such retardation that was previously unavailable. The Fisher-Rao gradient flow—which uses Fisher information as the *metric* rather than as an additive objective [9]—does not exhibit this interference, reinforcing the design principle below. In score-based diffusion [10], Fisher geometry similarly enters the score metric rather than the free energy, avoiding the paradox by construction.

In geometric frameworks where Fisher information enters the metric of the update rule rather than the objective functional, this interference does not arise [4, 5, 9]. This establishes a structural design principle: *geometric regularizers must be isolated to the update operator (metric tensor) rather than conflated with the global transport objective*. Conflating the two channels induces the thermodynamic delay and equilibrium shift quantified here.

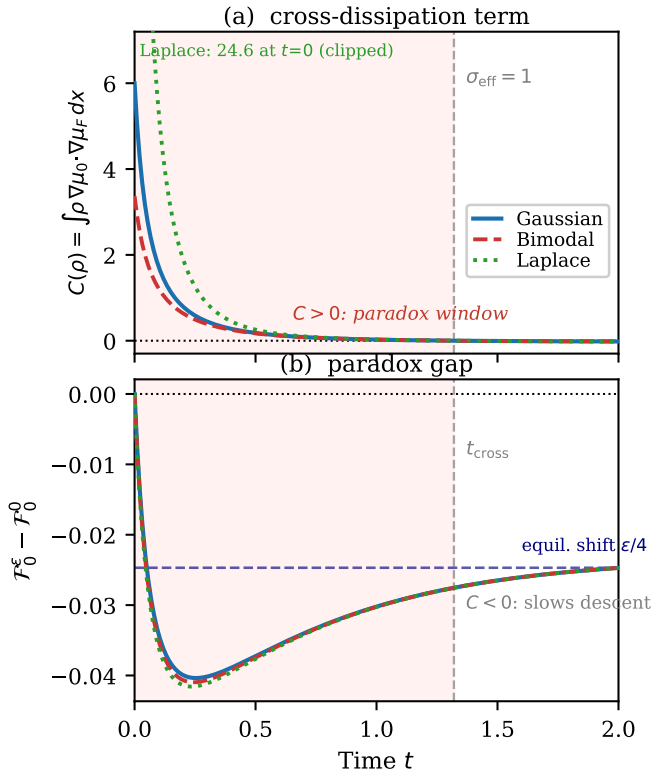


FIG. 4. Non-Gaussian validation of the Fisher Paradox ($\varepsilon = 0.1$, $\sigma_{\text{eff}} = 0.5$). (a) Cross-dissipation term $C(\rho(t)) = \int \rho \nabla \mu_0 \cdot \nabla \mu_F dx$ for Gaussian (solid), bimodal mixture (dashed), and Laplace (dotted) initial conditions. All three remain positive (paradox window, shaded) while $\sigma_{\text{eff}} < 1$, with identical crossing at $t_{\text{cross}} \approx 1.32$; the Laplace cusp spikes to 24.6 at $t=0$ ($\approx 4 \times$ the Gaussian value of 6.0; clipped; annotated). (b) Paradox gap $F_0^\varepsilon - F_0^0$. The gap is negative throughout (regularized system descends \mathcal{F}_0 faster while $C > 0$, then slower once $C < 0$ after t_{cross}) and settles to a permanent offset set by the equilibrium shift $\sigma_\infty = 1 + \varepsilon/4$. All three initial conditions converge to the same attractor.

The Fisher Paradox therefore reveals a previously unrecognized constraint on information-geometric gradient flows: stabilizing information channels can transiently oppose free-energy descent when curvature exceeds a critical scale.

M.F. developed the theoretical framework; A.K. performed the numerical simulations; Y.L. contributed to validation and manuscript preparation.

REFERENCES

- [1] R. Jordan, D. Kinderlehrer, and F. Otto, *SIAM Journal on Mathematical Analysis* **29**, 1 (1998).
- [2] F. Otto, *Communications in Partial Differential Equations* **26**, 101 (2001).
- [3] C. Villani, *Topics in Optimal Transportation* (American Mathematical Society, Providence, RI, 2003).
- [4] S.-i. Amari, *Neural Computation* **10**, 251 (1998).

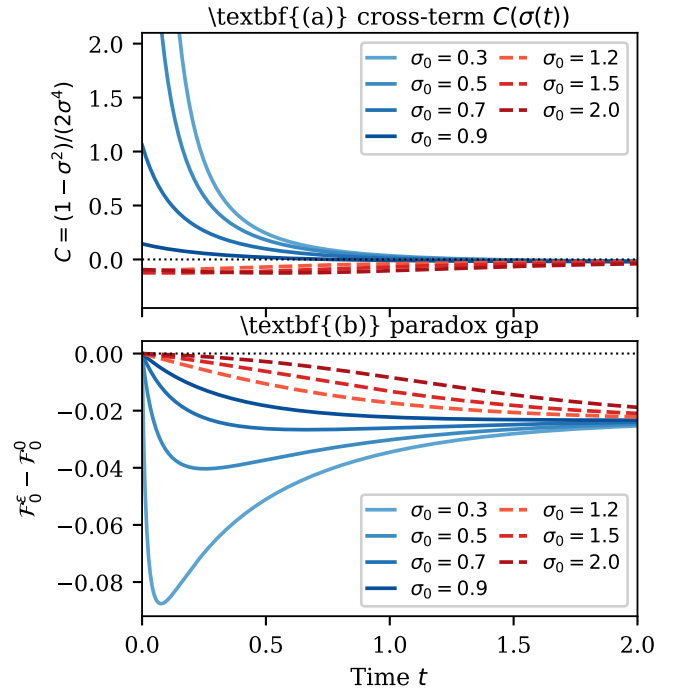


FIG. 5. Paradox dependence on $\sigma_0 \in [0.3, 2.0]$ ($\varepsilon = 0.1$). (a) Cross-term $C(\sigma(t)) = (1 - \sigma^2)/(2\sigma^4)$; blue curves ($\sigma_0 < 1$) are positive initially (paradox active), red curves ($\sigma_0 > 1$) negative. (b) Paradox gap $F_0^\varepsilon - F_0^0$; negative for $\sigma_0 < 1$ (retarded free-energy descent), positive for $\sigma_0 > 1$ (Fisher accelerates dissipation).

- [5] J. Martens, *Journal of Machine Learning Research* **21**, 1 (2020).
- [6] M. L. Mehta, *Random Matrices*, 3rd ed. (Elsevier, Amsterdam, 2004).
- [7] E. Madelung, *Zeitschrift für Physik* **40**, 322 (1927).
- [8] D. Bohm, *Physical Review* **85**, 166 (1952).
- [9] T. O. Gallouët and L. Monsaingeon, *ESAIM: Mathematical Modelling and Numerical Analysis* **51**, 2237 (2017).
- [10] Y. Song, J. Sohl-Dickstein, D. P. Kingma, A. Kumar, S. Ermon, and B. Poole, in *International Conference on Learning Representations (ICLR)* (2021).

SUPPLEMENTAL MATERIAL

This Supplemental Material provides complete derivations (Secs. A–F), and full details of the non-Gaussian robustness study including numerical method, initial conditions, cross-term diagnostics, paradox duration, and extended figures (Secs. S1–S6). Throughout, $\sigma_{\text{eff}}^2(t) = \int x^2 \rho(x, t) dx$ denotes the second moment of the distribution; for Gaussian states it coincides with the variance parameter σ^2 .

A.; FIRST VARIATION OF THE FISHER FUNCTIONAL

We use the convention

$$\Phi_F(\rho) = \int_{\mathbb{R}} |\partial_x \sqrt{\rho}|^2 dx = \frac{1}{4} I(\rho), \quad (\text{S1})$$

where $I(\rho) = \int \rho |\partial_x \log \rho|^2 dx$ is the standard Fisher information.

Set $f = \sqrt{\rho}$, so $\rho = f^2$ and $\Phi_F = \int f_x^2 dx$. For a mass-preserving variation $\rho_\eta = \rho + \eta h$ ($\int h dx = 0$, h smooth with rapid decay),

$$\delta f = \left. \frac{d}{d\eta} \right|_{\eta=0} \sqrt{\rho + \eta h} = \frac{h}{2f}. \quad (\text{S2})$$

Hence

$$\begin{aligned} \delta \Phi_F &= 2 \int f_x (\delta f)_x dx = 2 \int f_x \partial_x \left(\frac{h}{2f} \right) dx \\ &= -2 \int f_{xx} \frac{h}{2f} dx = - \int \frac{f_{xx}}{f} h dx, \end{aligned} \quad (\text{S3})$$

where integration by parts was applied in the last step. Therefore

$$\boxed{\frac{\delta \Phi_F}{\delta \rho} = - \frac{\partial_{xx} \sqrt{\rho}}{\sqrt{\rho}} \equiv \mu_F.} \quad (\text{S4})$$

Note that both factors of 2 cancel: the 2 in $2 \int f_x (\delta f)_x$ and the $\frac{1}{2}$ in $\delta f = h/(2f)$. This is the definition of μ_F used as Eq. (3) of the main letter.

For reference, the OU free energy gives

$$\mu_0 = \frac{\delta F_0}{\delta \rho} = \ln \rho + \frac{x^2}{2} + 1. \quad (\text{S5})$$

The additive constant is irrelevant because only $\nabla \mu_0$ enters the flow; we write $\mu_0 = \ln \rho + x^2/2$.

The regularized Fokker–Planck equation is therefore

$$\partial_t \rho = \partial_x \left[\rho \partial_x \left(\ln \rho + \frac{x^2}{2} - \varepsilon \frac{\partial_{xx} \sqrt{\rho}}{\sqrt{\rho}} \right) \right]. \quad (\text{S6})$$

B.; GAUSSIAN EVALUATION

Restrict to the Gaussian family $\rho_\sigma(x) = (2\pi\sigma^2)^{-1/2} \exp(-x^2/2\sigma^2)$. Then

$$\partial_{xx} \sqrt{\rho_\sigma} = \left(-\frac{1}{2\sigma^2} + \frac{x^2}{4\sigma^4} \right) \sqrt{\rho_\sigma}, \quad (\text{S7})$$

so

$$\boxed{\mu_F(x) = \frac{2\sigma^2 - x^2}{4\sigma^4}.} \quad (\text{S8})$$

The spatial gradients needed below are

$$\partial_x \mu_0 = x \left(1 - \frac{1}{\sigma^2} \right), \quad \partial_x \mu_F = -\frac{x}{2\sigma^4}. \quad (\text{S9})$$

C.; EXACT VARIANCE EQUATION ON THE GAUSSIAN MANIFOLD

Let $u(t) = \int x^2 \rho(x, t) dx = \sigma^2(t)$. Then

$$\dot{u} = -2 \int x \rho \partial_x \mu dx = -2 \int x \rho \partial_x \mu_0 dx - 2\varepsilon \int x \rho \partial_x \mu_F dx. \quad (\text{S10})$$

OU contribution. Using Eq. (S9) and $\int x^2 \rho_\sigma dx = \sigma^2$,

$$-2 \int x \rho \partial_x \mu_0 dx = -2 \left(1 - \frac{1}{\sigma^2} \right) \sigma^2 = 2(1 - \sigma^2). \quad (\text{S11})$$

Fisher contribution.

$$-2\varepsilon \int x \rho \partial_x \mu_F dx = \frac{\varepsilon}{\sigma^4} \int x^2 \rho_\sigma dx = \frac{\varepsilon}{\sigma^2}. \quad (\text{S12})$$

Combining, with $u = \sigma^2$,

$$\boxed{\dot{u} = 2(1 - u) + \frac{\varepsilon}{u}, \quad \dot{\sigma} = \frac{1 - \sigma^2}{\sigma} + \frac{\varepsilon}{2\sigma^3}.} \quad (\text{S13})$$

These are Eqs. (4)–(5) of the main text.

D.; EFFECTIVE POTENTIAL AND EQUILIBRIUM

Equation (S13) is a gradient flow:

$$\dot{u} = -V'(u), \quad V(u) = u^2 - 2u - \varepsilon \ln u. \quad (\text{S14})$$

The equilibrium $\dot{u} = 0$ satisfies $2u^2 - 2u - \varepsilon = 0$, giving

$$u_* = \frac{1 + \sqrt{1 + 2\varepsilon}}{2}, \quad \sigma_* = \sqrt{u_*} = 1 + \frac{\varepsilon}{4} + O(\varepsilon^2). \quad (\text{S15})$$

E.; DISSIPATION IDENTITY AND EXACT CROSS-TERM

The baseline free-energy time derivative is

$$\frac{dF_0}{dt} = \int \mu_0 \partial_t \rho dx = - \int \rho |\partial_x \mu_0|^2 dx - \varepsilon \int \rho \partial_x \mu_0 \cdot \partial_x \mu_F dx. \quad (\text{S16})$$

Define the Gaussian cross-term

$$C(\sigma) = \int \rho_\sigma \partial_x \mu_0 \cdot \partial_x \mu_F dx. \quad (\text{S17})$$

Substituting Eq. (S9),

$$\begin{aligned} C(\sigma) &= \int \rho_\sigma \cdot x \left(1 - \frac{1}{\sigma^2}\right) \cdot \left(-\frac{x}{2\sigma^4}\right) dx \\ &= -\frac{1}{2\sigma^4} \left(1 - \frac{1}{\sigma^2}\right) \sigma^2 = -\frac{\sigma^2 - 1}{2\sigma^4}. \end{aligned} \quad (\text{S18})$$

Therefore

$$\boxed{C(\sigma) = \frac{1 - \sigma^2}{2\sigma^4}}, \quad (\text{S19})$$

and the full dissipation identity is

$$\frac{dF_0}{dt} = -\frac{(\sigma^2 - 1)^2}{\sigma^2} - \varepsilon \frac{1 - \sigma^2}{2\sigma^4}. \quad (\text{S20})$$

In particular $C(\sigma) > 0$ for $\sigma \in (0, 1)$, $C(1) = 0$, and $C(\sigma) < 0$ for $\sigma > 1$, establishing the paradox window $0 < \sigma < 1$.

F.; CROSSING-TIME REPRESENTATION AND KL SCALING

Separating variables in Eq. (S13),

$$\boxed{t_{\text{cross}} = \int_{u_0}^1 \frac{u du}{2(u - u^2) + \varepsilon}}. \quad (\text{S21})$$

For $\varepsilon \rightarrow 0$,

$$t_{\text{cross}} \approx \frac{1}{2} \int_{u_0}^1 \frac{du}{1 - u} = \frac{1}{2} \ln \frac{1}{\sigma_0^2}. \quad (\text{S22})$$

The KL divergence between two zero-mean Gaussians is

$$D_{\text{KL}}(\rho_{\sigma_0} \parallel \rho_1) = \frac{1}{2} (\sigma_0^2 - 1 - \ln \sigma_0^2) \approx -\frac{1}{2} \ln \sigma_0^2, \quad \sigma_0 \ll 1, \quad (\text{S23})$$

giving the asymptotic scaling

$$t_{\text{cross}} \sim D_{\text{KL}}(\rho_{\sigma_0} \parallel \rho_1) \quad (\text{S24})$$

at leading order in ε and $\sigma_0 \ll 1$.

S1.; NUMERICAL METHOD

We solve the regularized Fokker–Planck equation

$$\partial_t \rho = \partial_x \left[\rho \partial_x \left(\ln \rho + \frac{x^2}{2} - \varepsilon \frac{\partial_{xx} \sqrt{\rho}}{\sqrt{\rho}} \right) \right] \quad (\text{S25})$$

on a uniform grid of $N = 512$ points on $[-8, 8]$ with periodic boundary conditions and spatial resolution $\Delta x = 16/512 \approx 0.031$. Time integration uses a semi-implicit operator-splitting scheme with step size $\Delta t = 10^{-4}$: the linear diffusion and drift terms are handled implicitly via tridiagonal solve, while the nonlinear Fisher term is treated explicitly. The cross-term $C(\rho(t))$ and effective variance $\sigma_{\text{eff}}^2(t) = \int x^2 \rho dx$ are computed at each step by direct quadrature. All three initial conditions used $\varepsilon = 0.1$.

Trajectory validation. For the Gaussian initial condition, the PDE-evolved $\sigma_{\text{eff}}(t)$ was compared against the ODE solution of $\dot{u} = 2(1 - u) + \varepsilon/u$ at 500 time points over $t \in [0, 3]$. The mean relative error is 5.21×10^{-4} , and the pointwise maximum relative error is 0.2%, confirming that the Gaussian closure is exact to numerical precision for this family of initial conditions.

S2.; INITIAL CONDITIONS

All initial conditions are normalized and matched to $\sigma_{\text{eff}} = 0.5$.

Gaussian. $\rho_0 = \mathcal{N}(0, 0.25)$.

Bimodal Gaussian mixture.

$$\rho_0(x) = \frac{1}{2} \mathcal{N}(-0.4, 0.09) + \frac{1}{2} \mathcal{N}(+0.4, 0.09). \quad (\text{S26})$$

The mode separation is 0.8 and each component has variance 0.09; the mixture variance is $0.09 + 0.16 = 0.25$, giving $\sigma_{\text{eff}} = 0.5$.

Laplace.

$$\rho_0(x) = \frac{1}{2b} e^{-|x|/b}, \quad b = \frac{\sigma_{\text{eff}}}{\sqrt{2}} \approx 0.354. \quad (\text{S27})$$

The Laplace variance is $2b^2 = \sigma_{\text{eff}}^2 = 0.25$. The sharp cusp at $x = 0$ produces a large Fisher information density and consequently a large initial cross-term (see Sec. S3).

S3. CROSS-TERM DIAGNOSTICS AT $t = 0$

The initial cross-term values $C(0) = \int \rho_0 \nabla \mu_0 \cdot \nabla \mu_F dx$ are tabulated below. All are positive, confirming paradox activation for all three distributions. The Gaussian value $C(0) = 6.0$ agrees with the analytical formula $C(\sigma_0) = (1 - \sigma_0^2)/(2\sigma_0^4) = (1 - 0.25)/(2 \times 0.0625) = 6.0$.

Distribution	$C(0)$	Ratio to Gaussian
Gaussian	6.00	1.0×
Bimodal mixture	3.37	0.56×
Laplace	24.65	4.1×

The elevated Laplace value reflects the $|x|$ -cusp: the Fisher term $\mu_F = -\partial_{xx}\sqrt{\rho}/\sqrt{\rho}$ diverges at the cusp, producing a large initial Fisher information density. The bimodal value is below the Gaussian because the inter-mode valley reduces the local gradient product relative to a unimodal distribution at the same σ_{eff} . Despite the four-fold Laplace amplification, all three trajectories converge to near-identical cross-term dynamics once σ_{eff} enters the competition window (Fig. S1).

S4.; PARADOX DURATION ACROSS DISTRIBUTIONS

The paradox crossing time (when σ_{eff} passes through 1 and C changes sign) is measured numerically as:

Distribution	t_{cross}
Gaussian	1.32
Bimodal mixture	1.32
Laplace	1.32

All three match to the resolution of the numerical integration. The theoretical prediction from the KL scaling law, $t_{\text{cross}} \sim \frac{1}{2} \ln(1/\sigma_0^2) = \frac{1}{2} \ln(1/0.25) \approx 0.69$ (small- ε limit), gives the correct order of magnitude; the exact value at $\varepsilon = 0.1$ from the integral formula is $t_{\text{cross}} \approx 1.32$, in agreement with all three numerical experiments. The identical crossing time across initial conditions reflects the fact that t_{cross} is controlled by the same effective D_{KL} to equilibrium, independent of the initial shape of ρ_0 .

S5.; EXTENDED NON-GAUSSIAN FIGURE

Figure S1 shows the complete three-panel diagnostic. Panel (a) displays the three initial conditions against the target $\mathcal{N}(0, 1)$. Panel (b) shows the cross-term trajectory: the Laplace spike decays within $t \lesssim 0.1$ and all three converge to near-identical dynamics through the competition window. Panel (c) shows $\mathcal{F}_0(\rho(t))$ for Fisher-regularized (dashed) versus baseline (solid) flows; all three regularized trajectories reach the same shifted attractor $\sigma_\infty \approx 1 + \varepsilon/4$ (Sec. D).

Figure S2 shows the full energy decomposition for the Gaussian case, displaying \mathcal{F}_ε , \mathcal{F}_0 , and $\varepsilon\Phi_F$ as separate curves.

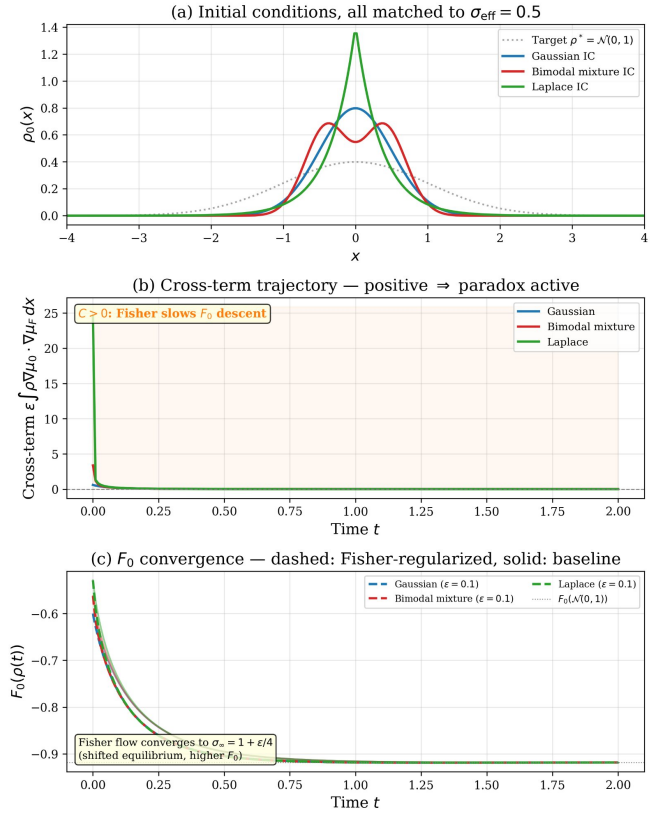


FIG. S1. Extended non-Gaussian validation ($\varepsilon = 0.1$, $\sigma_{\text{eff}} = 0.5$). (a) Initial conditions: Gaussian (blue), bimodal mixture (red), and Laplace (green), all matched to $\sigma_{\text{eff}} = 0.5$, against target $\mathcal{N}(0, 1)$ (dotted). (b) Cross-term trajectory; the Laplace cusp produces an initial spike ($C(0) \approx 24.65$) that decays rapidly; all three converge to the same dynamics in the competition window. (c) Baseline free energy $\mathcal{F}_0(\rho(t))$ for Fisher-regularized (dashed) vs. baseline (solid) flows. All three regularized curves settle at the same shifted attractor, confirming the equilibrium prediction $\sigma_\infty = 1 + \varepsilon/4$ (annotation).

S6. ASYMPTOTIC BOUND ON NON-GAUSSIAN CORRECTION TO t_{cross}

The variance moment equation for an arbitrary (non-Gaussian) ρ is

$$\dot{u} = 2(1 - u) + \varepsilon K(\rho), \quad u = \sigma_{\text{eff}}^2, \quad (\text{S28})$$

where the Fisher variance moment is

$$K(\rho) = -2 \int x \rho \partial_x \mu_F dx. \quad (\text{S29})$$

This is distinct from the free-energy cross-term $C(\rho) = \int \rho \partial_x \mu_0 \cdot \partial_x \mu_F dx$ appearing in the dissipation identity. For a Gaussian state $K_G(\sigma) = 1/\sigma^2 = 1/u$, recovering Eq. (5) of the main text.

Write $K(\rho) = K_G(u) + \delta K(\rho)$, where δK captures shape-dependent deviations. Expanding t_{cross} in ε , the

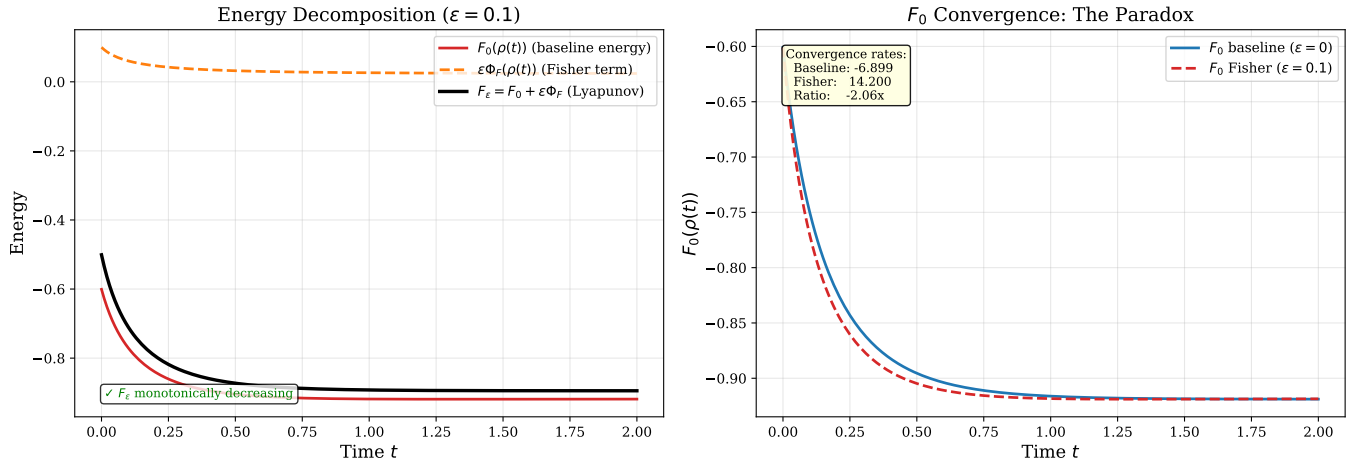


FIG. S2. Full energy decomposition ($\epsilon = 0.1$, Gaussian initial condition). *Left*: Lyapunov functional \mathcal{F}_ϵ (black) decreases monotonically while \mathcal{F}_0 (red) and $\epsilon\Phi_F$ (orange dashed) compete transiently. *Right*: Paradox detail—Fisher-regularized \mathcal{F}_0 (dashed red) converges at $-2.06\times$ the unregularized baseline rate (solid blue) during the competition window.

non-Gaussian correction satisfies

$$|\Delta t_{\text{cross}}| \leq \epsilon \int_0^{t_{\text{cross}}} \frac{|\delta K(\rho(t))|}{(\dot{u})^2} |\dot{u}| dt. \quad (\text{S30})$$

For the leading-order estimate, $|\delta K_0/K_G| \sim \kappa_4/\sigma^4$ where κ_4 is the fourth cumulant of ρ_0 . For the Laplace initial condition ($b = 0.354$): $\kappa_4 = 6b^4 \approx 0.094$, $\sigma^4 = 0.0625$, giving $|\delta K_0/K_G| \approx 1.5$.

The shape-dependent correction $\delta K(\rho(t))$ decays on the OU shape-relaxation timescale. The leading OU eigenvalue for shape relaxation is $\lambda_2 = 2$ (the second Hermite mode), giving $|\delta K(\rho(t))| \lesssim |\delta K_0|e^{-2t}$. Inserting this into the bound (S30) and evaluating at the initial

rate $\dot{u}|_{t=0} = 2(1 - u_0) + \epsilon/u_0$,

$$|\Delta t_{\text{cross}}| \leq \frac{\epsilon |\delta K_0|}{\dot{u}|_{t=0}} \int_0^\infty e^{-2t} dt = \frac{\epsilon |\delta K_0|}{2 \dot{u}|_{t=0}}. \quad (\text{S31})$$

For the Laplace case with $u_0 = 0.25$, $\epsilon = 0.1$:

$$|\Delta t_{\text{cross}}| \leq \frac{0.1 \times 1.5 \times (1/0.25)}{2 \times 1.90} = 0.079, \quad (\text{S32})$$

which is $\approx 6\%$ of $t_{\text{cross}} \approx 1.32$. This is an upper bound; near $u \rightarrow 1$ where the integrand in $t_{\text{cross}} = \int_{u_0}^1 u du / [2(u - u^2) + \epsilon]$ is concentrated, $\dot{u} \rightarrow 0^+$ and ρ has already relaxed toward Gaussian (shape-relaxation rate 2 exceeds variance rate \dot{u} throughout most of $[0, t_{\text{cross}}]$), so the actual correction is smaller than the bound.

The bound implies $|\Delta t_{\text{cross}}| \lesssim 0.08$, or roughly 6% of $t_{\text{cross}} \approx 1.32$, consistent with the numerical observations in Table S4 (Sec. S4).